Sub-picosecond exchange–relaxation in the compensated ferrimagnet Mn_2Ru_xGa

OPEN ACCESS
IOP Publishing
Journal of Physics: Condensed Matter
J. Phys.: Condens. Matter **33** (2021) 135804 (6pp)
https://doi.org/10.1088/1361-648X/abda7c

Sub-picosecond exchange–relaxation in the compensated ferrimagnet Mn_2Ru_xGa

G Bonfiglio[1,*], K Rode[2], G Y P Atcheson[2], P Stamenov[2], J M D Coey[2], A V Kimel[1], Th Rasing[1] and A Kirilyuk[1,3]

[1] Radboud University, Institute for Molecules and Materials, 6525 AJ Nijmegen, The Netherlands
[2] CRANN, AMBER and School of Physics, Trinity College Dublin, Ireland
[3] FELIX Laboratory, Radboud University, Toernooiveld 7, 6525 ED Nijmegen, The Netherlands

E-mail: g.bonfiglio@science.ru.nl

Received 10 November 2020, revised 20 December 2020
Accepted for publication 11 January 2021
Published 29 January 2021

Abstract

We study the demagnetization dynamics of the fully compensated half-metallic ferrimagnet Mn_2Ru_xGa. While the two antiferromagnetically coupled sublattices are both composed of manganese, they exhibit different temperature dependencies due to their differing local environments. The sublattice magnetization dynamics triggered by femtosecond laser pulses are studied to reveal the roles played by the spin and intersublattice exchange. We find a two-step demagnetization process, similar to the well-established case of $Gd(FeCo)_3$, where on a 5 ps timescale the two Mn-sublattices seem to have different demagnetization rates. The behaviour is analysed using a four-temperature model, assigning different temperatures to the two manganese spin baths. Even in this strongly exchange-coupled system, the two spin reservoirs have considerably different behaviour. The half-metallic nature and strong exchange coupling of Mn_2Ru_xGa lead to spin angular momentum conservation at much shorter time scales than found for $Gd(FeCo)_3$ which suggests that low-power, sub-picosecond switching of the net moment of Mn_2Ru_xGa is possible.

Keywords: ultrafast magnetization dynamics, ferrimagnet, Heusler alloy, all-optical switching, spin dynamics

(Some figures may appear in colour only in the online journal)

Beaurepaire *et al* [1] demonstrated in 1996 that the magnetization of a ferromagnet can be changed on the sub-picosecond timescale thereby raising the possibility that the combination of magnetism and light may bridge the 'terahertz gap' in spin electronic devices. Further striking observations were made a few years later when short laser pulses were shown to switch the net magnetization of a ferrimagnet. This is now called all-optical switching (AOS) [2–4]. The best-studied AOS material is the amorphous compensated ferrimagnet $Gd(FeCo)_3$ where toggle switching can be understood by allowing for exchange of angular momentum between the Gd and FeCo sublattices due to exchange interaction between them [5–7]. The fundamentals of AOS have been subject to intense investigation since then, and several different models [7–10] have been put forward, all based on transfer of energy and angular momentum between the electronic, lattice and spin subsystems. In order to understand the dynamics of switching, exchange, electron–phonon interaction and spin–lattice relaxation must all be considered [10]. The key feature of all the models however, is different relaxation dynamics for the two sublattices. The Gd and transition metal spin reservoirs must be described separately, adding one extra temperature [11] to the widely accepted, phenomenological, three-temperature model (3TM) [1] for a ferromagnet. This four-temperature description (4TM), reproduces the demagnetization dynamics of these

* Author to whom any correspondence should be addressed.

alloys quite well, indirectly validating different demagnetization dynamics for the two sublattices, as was observed by XMCD [5]. It was shown by Mangin *et al* [12] that all-optical influence on the magnetization can be achieved in various structures: alloys, multilayers, heterostructure and rare-earth-free synthetic ferrimagnets. From those results it was possible to infer three empirical design rules for a ferrimagnet to show AOS: antiferromagnetic coupling, non-equivalent sublattices and perpendicular anisotropy [13]. In this respect, a yet unexplored and fascinating new material for AOS is the ferrimagnetic half-metal Mn_2Ru_xGa [14] (MRG). Due to its half-metallicity, it could be an ideal material for spintronic devices [15–17]. The two antiferromagnetically coupled sublattices, both Mn-based, present different temperature dependencies of their magnetizations due to the different local electronic environment at the two different crystallographic sites (4*c* and 4*a* positions in the $F\bar{4}3m$ space group, both with four Mn atoms) [18]. At low temperature, their magnetizations are approximately 547 and 585 k Am^{-1} for the 4*a* and 4*c* sublattices [19]. There is a spin gap in one sublattice of about 1 eV, and the electrons at the Fermi level in the other subband belong predominantly to the 4*c* sublattice [14], as shown in inset in figure 2. We have shown that the laser-induced spin precession resembles that of a ferromagnet, but with much higher frequency and relatively low damping [20].

Recently, Banerjee *et al* [21] have shown that MRG exhibits single-pulse all-optical toggle switching that is both similar to and very different from $Gd(FeCo)_3$. In particular, the two Mn sublattices are strongly (compared to $Gd(FeCo)_3$) exchange-coupled [19] and of the same magnitude. Unlike $Gd(FeCo)_3$, the differing sublattice demagnetization rates cannot be determined entirely by the sublattice moments and their angular momenta. It must therefore be driven by angular momentum *conservation* and inter-sublattice exchange relaxation, as recently discussed by Davies *et al* [22] who inferred the coupled character of the sublattice dynamics from the static switching dependence on temperature and Ru concentration. The question is if the spin-resolved heat capacity, determined almost entirely by the spin-polarized density of states at the Fermi level, is sufficiently distinct to account for the substantial difference in characteristic demagnetization times. Are the two spin reservoirs in equilibrium with each other during the entire de- and re-magnetization?

In order to answer this question, we study the demagnetization dynamics of MRG in applied magnetic fields of up to 7 T. The initial ultrafast (less than 1 ps) demagnetization is followed by a plateau or a remagnetization, and a slower demagnetization process after this. We will show that numerical simulations based on the 4TM reproduce the experimental data, and provide us with a set of intrinsic material parameters that help understand the ultrafast behaviour of MRG. The relatively strong inter-sublattice exchange interaction leads to overall faster dynamics of MRG than has been observed for $Gd(FeCo)_3$.

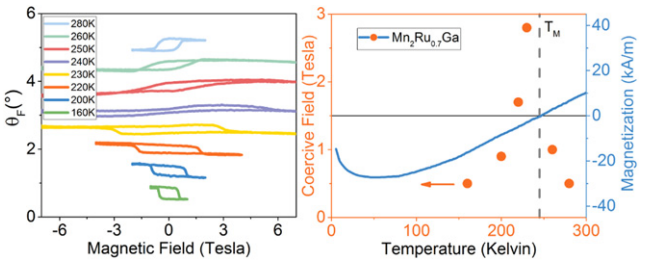

Figure 1. (Left) hysteresis loops recorded via Faraday rotation measurements using an 800 nm continuous wave laser. The coercive field measured at 240 and 250 K in the left panel is not included in the right panel summary as the maximum available applied field (7 T) is insufficient to obtain a fully saturated state at these temperatures. (Right) net moment measured by SQUID magnetometry (in blue) and coercive field measured by static Faraday effect (orange). The upturn of the net moment below T ∼50 K is due to paramagnetic impurities in the MgO substrate. The magnetic compensation point, T_M, at ∼245 K is indicated with a dashed line, below this point the dominant sublattice is the 4*c* one. The magnetic field applied along the easy-axis is able to saturate the sample ∼15 K above or below T_M.

The ferrimagnetic Mn_2Ru_xGa sample used in these experiments has a magnetic compensation point $T_{comp} \sim 245$ K (see figure 1) and the Curie temperature is $T_C \sim 550$ K.

Thin films of MRG were grown on MgO (001) substrates in a 'Shamrock' sputter deposition cluster with a base pressure of 2×10^{-8} Torr. The substrate was kept at 250 °C during deposition of MRG, and a protective, ∼3 nm, layer of aluminium oxide was added post-deposition at room temperature. Further information on sample deposition can be found elsewhere [18]. The thickness of the sample is 50 nm and $x = 0.7$.

The demagnetization dynamics were investigated using a two-colour pump–probe scheme in a Faraday geometry inside a $\mu_0 H_{max} = 7$ T superconducting magnet. Data shown were recorded below T_{comp} at 210 K and 230 K. Both pump and probe were produced by a Ti:sapphire femtosecond pulsed laser amplifier with a central wavelength of 800 nm, a pulse width of 40 fs and a repetition rate of 1 kHz. The beam was split in two parts, with the high-intensity one frequency doubled by a BBO crystal (producing $\lambda = 400$ nm) and used as a pump pulse. The lower-intensity part with the wavelength of 800 nm acted as the probe. The time delay between the two pulses was adjusted using a mechanical delay stage. To improve the signal-to-noise ratio, the pump pulses were modulated by a synchronized mechanical chopper at 500 Hz for subsequent lock-in detection. Both beams were linearly polarized, and with spot sizes on the sample of 150 μm and 70 μm for pump and probe, respectively. After interaction with the sample, the probe beam was split in two orthogonally polarized components using a Wollaston prism. The pump-induced changes in transmission and Faraday rotation were thus detected by measuring the sum and the difference in intensity of the two signals. We note that DC-heating of the sample due to the laser

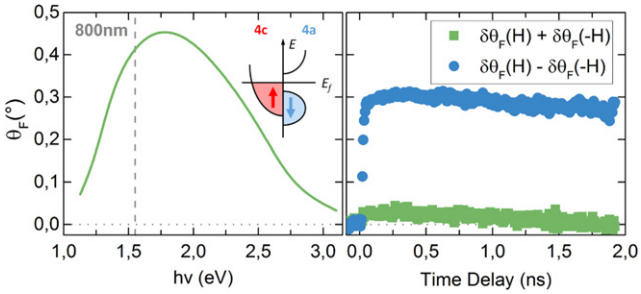

Figure 2. (Left) MRG Faraday rotation (θ_F) as a function of the photon energy. The dashed vertical line indicates the probe energy ($\lambda = 800$ nm) for magnetization dynamics hereafter. In the inset, a schematic representation of the band structure. (Right) pump induced changes of θ_F, indicated as $\delta\theta_F$. Green squares show effects that are even in applied field, while blue squares show odd ones. They are the sum and the difference of data obtained with positive and negative applied fields (± 3 T) at $T = 220$ K. Changes in transmission are small and negligible compared to the changes induced by magnetization dynamics.

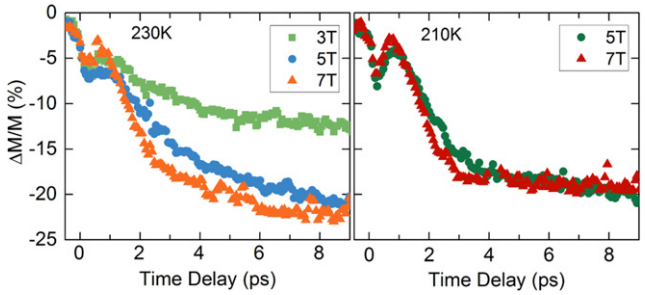

Figure 3. Demagnetization dynamics for three different fields at 230 K (left) and 210 K (right). Interestingly, the slow process depends on the applied field already at delay time >1 ps, while the fast one (sub 1 ps) does not.

is negligible and that, together with the external magnetic field applied along the easy axis (i.e. out of plane) to fully saturate the sample, the initial condition are restored between each pump pulse.

In figure 2 the magneto-optical spectrum of MRG is plotted from 1.12 eV to 3.1 eV. The photons with energy 1.55 eV probe mainly the 4*c* sublattice. The main contribution to the dielectric permittivity in the visible and near infrared arises from the Drude tail [23] so that the magneto-optical probe follows the behaviour of the highly spin-polarized conduction band. However, a rather large density of states in the vicinity of the spin gap indicates that excitation of 4*a* states is possible as well [24]. We note that the Faraday rotation does not change sign from 1 eV to 3 eV (figure 2), the hysteresis loops obtained by MOKE/Faraday match those obtained by anomalous Hall effect [20], and the anomalous Hall angle (ρ_{xy}/ρ_{xx}) almost perfectly matches the same ratio extrapolated from the optical measurements [23]. This indicates that the sublattice contributing most of the electrons close to the Fermi level is mostly responsible for the magneto-optical response at 800 nm and 400 nm.

The effect of a pump pulse with the fluence of 6.5 mJ cm^{-2} is shown in figure 2 for delay times up to 2 ns. As the polarity of the applied field is changed, we observe a reversed sign of the Faraday rotation. In the pump-induced dynamics we can distinguish effects that are odd and even in magnetic field from the difference and the sum (figure 2). The difference is assigned to the magnetization dynamics while the sum can be explained by time-dependent changes of transmission through the sample.

AOS generally proceeds in three different steps. First the ultrashort laser pulse leads to a drastic increase of the electronic temperature, above the magnetic ordering temperature T_C. Subsequently, heat is transferred from the hot electrons to the spin subsystem in around 1 ps, leading to rapid demagnetization. In the case where the atomic moments of the two sublattices are substantially different, as for GdCo, they will demagnetize with different characteristic times, proportional to μ_i/α_i, where μ_i is the sublattice atomic moment and α_i its damping constant [25, 26]. A transient ferromagnetic state arises, followed by complete switching of the magnetic order. An important part of this process is that angular momentum is exchanged between the sublattices, due to exchange relaxation [7], resulting in acceleration of the demagnetization for both sublattices.

In our experiment, the strong field applied along the easy axis ensures that when the system cools down (starting from few hundreds of picoseconds, figure 2) the initial magnetic state is restored.

The dynamics during the first 9 ps show that the demagnetization is non-monotonic, while after this time no further changes in the demagnetization are present. In figure 3 the first, field-independent, ultrafast demagnetization step happens within 200 fs of the pump pulse arrival, followed by a plateau or a small re-magnetization from 1 ps to 1.5 ps. After this transient state, the sample continues to demagnetize further, but at a slower rate dependent on the applied field.

This behaviour clearly resembles the demagnetizing dynamics of $Gd(FeCo)_3$, where the two sublattices demagnetize at different speeds due to both their different magnetic moments and strongly different intra-sublattice exchange constants. In the case of MRG the atomic moments of the Mn sublattices are almost equal [18] and, in addition, the exchange constants (both intra- and inter-sublattice) [19] are considerably stronger [6, 7, 22]. Thus, the demagnetization rates for the two sublattices are expected to be similar, which is clearly contradicted by the observation of a non-monotonic demagnetization process.

In order to understand this, we note that for a strongly coupled ferrimagnetic system, the effect of a short laser pulse is different from that in a simple ferromagnet. Indeed, due to the strong antiferromagnetic inter-sublattice exchange, the total spin angular momentum can be conserved by passing it from one sublattice to the other. However, the temperature dependencies of the two are strongly different, thus an equal change of momentum corresponds to a larger variation in effective temperature for the 4*c* sublattice than the 4*a*. We think this is the main reason for the emergence of a strongly non-equilibrium magnetic state in MRG.

In figure 3 we also show the dependence of the demagnetization process on the magnitude of the applied magnetic field.

Table 1. Parameters used for the 4TM. The second column shows values for GdCoFe [11].

Constants	Mn_2Ru_xGa	GdCoFe	Unit
γ_e	484	714	J m^{-3} K^{-2}
C_l	2.27×10^6	3×10^6	J m^{-3} K^{-1}
$C_{4a/Gd}$	2×10^5	0.65×10^5	J m^{-3} K^{-1}
$C_{4c/CoFe}$	0.3×10^4	1.3×10^4	J m^{-3} K^{-1}
G_{el}	8×10^{17}	2×10^{17}	J m^{-3} K^{-1}
$G_{es}^{4c/CoFe}$	2.8×10^{15}	1.3×10^{15}	W m^{-3} K^{-1}
$G_{es}^{4a/Gd}$	3×10^{15}	0.6×10^{15}	W m^{-3} K^{-1}
$G_{ls}^{4c/CoFe}$	3×10^{15}	4.8×10^{15}	W m^{-3} K^{-1}
$G_{ls}^{4a/Gd}$	9×10^{16}	0.23×10^{15}	W m^{-3} K^{-1}
G_{ss}	2.8×10^{16}	0.77×10^{15}	W m^{-3} K^{-1}

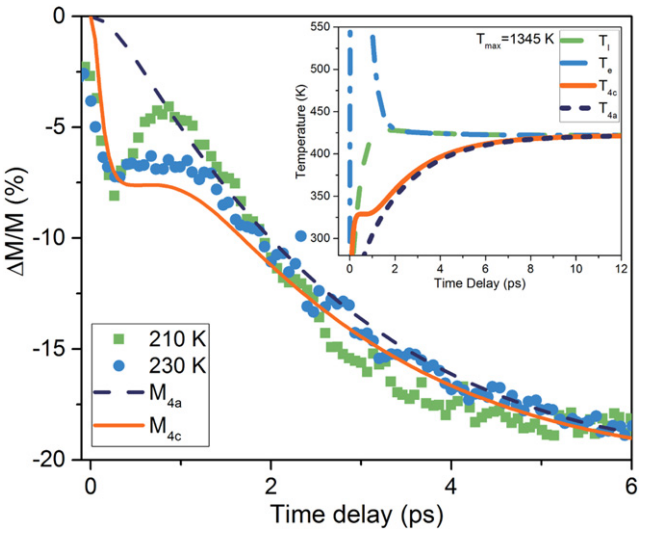

Figure 4. Laser-induced demagnetization in an applied field of 5 T. Thick lines are curves obtained from the 4TM. Inset: Time dependence of electron, lattice, 4*c* and 4*a* heat reservoirs. The electronic temperature increases above T_C following the laser excitation, and it cools down within 1 ps. It reaches equilibrium with the lattice within 2 ps. The temperature of the 4*c* and 4*a* sublattices strongly differ for the first 2 ps, after which they are in equilibrium.

An increase of the external field leads to a faster dynamics only for the second, slower part of the process, while the first step of demagnetization remains unaffected. The first part of the dynamics results field-insensitive due to the dominance of the exchange relaxation process following the spike in the electronic temperature, caused by the strong pump pulse—thus, both sublattices start to demagnetize. After the cool down, $t < 2$ ps, the magnetic system formed by the two sublattices regains its magnetic susceptibility, and is affected by the external magnetic field, accelerating the demagnetization dynamics. Between 2 ps to 4 ps in right panel of figure 3, we tentatively note two periods of a high-frequency oscillation, $f \sim 0.6$ THz to 1 THz which is in agreement with the frequency expected for the antiferromagnetic mode of MRG. Indeed, as reported elsewhere [27], a small in-plane component of the 4*a* sublattices is present and could be the reason of these small amplitude oscillations.

In order to model the different behaviour of the two Mn-sublattices, we performed calculations using the 4TM described above: four coupled differential equations that describe the effect of a laser pulse on the different heat baths. The interaction of the pump pulse with the sample is described as an increase of the electronic temperature, T_e, that follows the laser intensity profile. Then, the system thermalizes within 1–2 ps by redistributing the heat to different heat-baths, with different time constants for each subsystem. The lattice is considered as a phonon bath (T_l), while the two magnetic sublattices 4*a* and 4*c* are represented by two different temperatures—T_{4a} and T_{4c}, respectively.

Initially, we used the set of *G*-parameters of GdCoFe for the coupling constants [1, 28]. For the specific heat capacities of lattice and electron systems, C_l and C_e, we used values for Mn_2Ga single crystals [29], shown in table 1, where the heat capacity of the electron system is indicated trough $\gamma_e = C_e/T_e$—the proportionality factor. The solution of the system of equations thus gives us the time evolution of the temperatures of the different subsystems, i.e. electrons, lattice and the two spin sublattices.

Given the high number of unknown parameters we tentatively connect the values of coupling constants with the well-known properties of MRG. Thus providing some rough guess of these values for a qualitative analysis of the dynamics here observed. We therefore adjust each parameter manually to obtain a good agreement with the experimental results, while keeping in mind the peculiarities of the system. A difference in the heat capacity of the two spin subsystem, C_{4a} and C_{4c}, is expected due to their different electronic density of states [24]. In addition, the coupling constants can be qualitatively related to the strength of the magnetic exchange. We expect a strong spin-spin coupling (G_{ss}) and a stronger lattice–spin coupling for the 4*a* sublattice, G_{ls}^{4a}, compared to the 4*c* one.

Using the adjusted parameters, the electronic temperature, T_e [figure 4 (inset)], reaches 1345 K in roughly 100 fs, while the lattice and sublattices 4*c*/4*a* (T_l, T_{4c} and T_{4a} respectively) remain close to 350 K. The heat deposited in the electronic system is then redistributed between the other subsystems. In particular, within 2 ps the electronic and lattice subsystems are in thermal equilibrium. On the other hand, equilibration between both spin sublattices, from one side, and electrons and lattice, from the other side, takes ∼10 ps. This behaviour is quite similar to that of GdCoFe, but with one major difference. We note that the temperature of the two spin subsystems in MRG follow a similar relaxation path already at ∼2 ps, while for GdFeCo the relaxation times are quite different. As explained above, this suggests that the interplay of a strong exchange coupling between sublattices (inter-exchange) and the electronic structure of MRG leads to dynamics where the total spin angular momentum of the two sublattices is practically conserved after a very short time of ∼1 ps–2 ps.

To compare with experimental data, we converted the temperature-time dependencies following a $T^{3/2}$ Bloch law [1, 11] as the strong exchange keeps some amount of magnetic order even in the non-equilibrium state (see above). Figure 4 shows reasonable agreement between experimental data and the 4TM. In addition to the experimental data representing the

4*c* sublattice magnetization, we also show the 4*a* magnetization, inferred from the model, to highlight its strong influence on the demagnetization process. What we observe is an ultrafast demagnetization of one of the sublattices (assumed to be 4*c*), followed by a secular equilibrium (when the temperature of the measurement is 230 K) or by a fast remagnetization (at 210 K). As shown in the inset, directly after the arrival of the pump, the electronic temperature increases drastically, leading to a regime where the relaxation processes dominates the dynamics. After ∼1.5 ps the electronic temperature drops low enough so that the dynamics can now be driven by the exchange, thus allowing angular momentum to be exchanged between the two sublattices. As a consequence, the second step of the demagnetization is observed, that reaches its minimum after ∼10 ps.

Regarding the refined values of the 4TM parameters, we highlight two points. First, the coupling constant of the two magnetic sublattices is considerably stronger in MRG than for GdCoFe, as expected given the higher exchange coupling. Second, a strong difference is found in the heat capacity of the two sublattices. These values are in line with what could be expected from MRG with its two different manganese spin systems.

In conclusion, we have shown that a femtosecond pump pulse can demagnetize MRG in approximately 10 ps via a two-step process. This result is similar to what was already observed for amorphous GdCoFe alloys [11]. Surprisingly, here we observe a faster evolution of the demagnetization dynamics. Indeed, one of the sublattices (assumed to be 4*c*, based on earlier experiments and density functional theory [24]) demagnetizes in few hundred of fs, and at ∼1.5 ps a second demagnetization process starts, that is induced by the second sublattice (4*a*). We underline that the process observed here, and the apparent faster demagnetization of one sublattice, arises from the exchange-driven dynamics. This is supported by the similar demagnetization rate of Mn in the two sublattices and by the strong exchange in MRG.

We have modelled the experimental data, using the phenomenological 4TM model, thereby establishing, at least approximately, the intrinsic properties that govern not only demagnetization but also AOS. Additionally, we were able to demonstrate the essential differences between GdFeCo and MRG, which we believe will facilitate a future theoretical description of magnetization dynamics. We stress that, even though we only observe a partial demagnetization, these results highlight a pathway towards all-optical-switching in ferrimagnetic Heusler alloys. A faster demagnetization rate is essentially connected to faster heat-transfer and smaller heat capacity, that can lead to deterministic AOS of MRG with switching times as short as ∼1 ps when the two spin reservoirs achieve equilibrium.

Data availability statement

All data that support the findings of this study are included within the article (and any supplementary files).

Acknowledgments

This project has received funding from the NWO, the *European Union's* Horizon 2020 research and innovation programme under Grant Agreement No. 737038 'TRANSPIRE', as well as from Science Foundation Ireland through contracts 12/RC/2278 AMBER and 16/IA/4534 ZEMS

ORCID iDs

G Bonfiglio https://orcid.org/0000-0002-0688-8712
A Kirilyuk https://orcid.org/0000-0003-1479-9872

References

[1] Beaurepaire E, Merle J-C, Daunois A and Bigot J-Y 1996 *Phys. Rev. Lett.* **76** 4250
[2] Stanciu C D, Tsukamoto A, Kimel A V, Hansteen F, Kirilyuk A, Itoh A and Rasing T 2007 *Phys. Rev. Lett.* **99** 217204
[3] Lambert C-H *et al* 2014 *Science* **345** 1337
[4] Stupakiewicz A, Szerenos K, Afanasiev D, Kirilyuk A and Kimel A V 2017 *Nature* **542** 20807
[5] Radu I *et al* 2011 *Nature* **472** 09901
[6] Ostler T *et al* 2012 *Nat. Commun.* **3** 666
[7] Mentink J H, Hellsvik J, Afanasiev D V, Ivanov B A, Kirilyuk A, Kimel A V, Eriksson O, Katsnelson M I and Rasing T 2012 *Phys. Rev. Lett.* **108** 057202
[8] Atxitia U, Chubykalo-Fesenko O, Walowski J, Mann A and Münzenberg M 2010 *Phys. Rev.* B **81** 174401
[9] Cornelissen T D, Córdoba R and Koopmans B 2016 *Appl. Phys. Lett.* **108** 142405
[10] Gridnev V N 2018 *Phys. Rev.* B **98** 014427
[11] Mekonnen A *et al* 2013 *Phys. Rev.* B **87** 180406(R)
[12] Mangin S *et al* 2014 *Nat. Mater.* **13** 286
[13] Kimel A V 2014 *Nat. Mater.* **13** 225
[14] Kurt H, Rode K, Stamenov P, Venkatesan M, Lau Y C, Fonda E and Coey J M D 2014 *Phys. Rev. Lett.* **112** 027201
[15] Borisov K *et al* 2016 *Appl. Phys. Lett.* **108** 192407
[16] Borisov K, Atcheson G, D'Arcy G, Lau Y-C, Coey J M D and Rode K 2017 *Appl. Phys. Lett.* **111** 102403
[17] Thiyagarajah N, Lau Y-C, Betto D, Borisov K, Coey J M D, Stamenov P and Rode K 2015 *Appl. Phys. Lett.* **106** 122402
[18] Betto D, Thiyagarajah N, Lau Y-C, Piamonteze C, Arrio M-A, Stamenov P, Coey J M D and Rode K 2015 *Phys. Rev.* B **91** 094410
[19] Fowley C *et al* 2018 *Phys. Rev.* B **98** 220406(R)
[20] Bonfiglio G *et al* 2019 *Phys. Rev.* B **100** 104438
[21] Banerjee C, Teichert N, Siewierska K, Gercsi Z, Atcheson G, Stamenov P, Rode K, Coey J M D and Besbas J 2020 *Nat. Commun.* **11** 4444
[22] Davies C S, Janssen T, Mentink J H, Tsukamoto A, Kimel A V, van der Meer A F G, Stupakiewicz A and Kirilyuk A 2020 *Phys. Rev. Appl.* **13** 024064
[23] Fleischer K, Thiyagarajah N, Lau Y-C, Betto D, Borisov K, Smith C C, Shvets I V, Coey J M D and Rode K 2018 *Phys. Rev.* B **98** 134445
[24] Žic M *et al* 2016 *Phys. Rev.* B **93** 140202(R)
[25] Koopmans B, Ruigrok J J M, Longa F D and de Jonge W J M 2005 *Phys. Rev. Lett.* **95** 267207
[26] Koopmans B, Malinowski G, Dalla Longa F, Steiauf D, Fähnle M, Roth T, Cinchetti M and Aeschlimann M 2010 *Nat. Mater.* **9** 259
[27] Siewierska K E, Atcheson G, Borisov K, Venkatesan M, Rode K and Coey J M D 2017 *IEEE Trans. Magn.* **53** 1

[28] Seixas T M, Salgueiro da Silva M A, de Lima O F, Lopez J, Braun H F and Eska G 2010 *J. Phys.: Condens. Matter* **22** 136002

[29] Winterlik J, Balke B, Fecher G H, Felser C, Alves M C M, Bernardi F and Morais J 2008 *Phys. Rev.* B **77** 054406